Saringer, C.; Tkadletz, M.; Stark, A.; Schell, N.; Czettl, C.; Schalk, N.:
In-situ investigation of the oxidation behavior of metastable CVD-Ti1-xAlxN using a novel combination of synchrotron radiation XRD and DSC.
In: Surface and Coatings Technology. Vol. 374 (2019) 617 - 624.
First published online by Elsevier: 27.05.2019

https://dx.doi.org/10.1016/j.surfcoat.2019.05.072

In-situ investigation of the oxidation behavior of metastable CVD $Ti_{1-x}Al_xN$ using a novel combination of synchrotron radiation XRD and DSC

Christian Saringer [a,*], Michael Tkadletz [b], Andreas Stark [c], Norbert Schell [c], Christoph Czettl [d], Nina Schalk [a]

[a] Christian Doppler Laboratory for Advanced Coated Cutting Tools at the Department of Materials Science, Montanuniversität Leoben, Franz-Josef-Strasse 18, 8700 Leoben, Austria
[b] Department of Materials Science, Montanuniversität Leoben, Franz-Josef-Strasse 18, 8700 Leoben, Austria
[c] Institute of Materials Research, Helmholtz-Zentrum Geesthacht, Max-Planck-Strasse 1, 21502, Geesthacht, Germany
[d] Ceratizit Austria GmbH, Metallwerk-Plansee-Strasse 71, 6600 Reutte, Austria

Email: christian.saringer@unileoben.ac.at

Keywords: in situ, synchrotron radiation, oxidation, phase composition, chemical vapor deposition; TiAlN

Abstract

$Ti_{1-x}Al_xN$ hard coatings deposited by chemical vapor deposition (CVD) have attracted much attention recently due to their extraordinary nanolamellar microstructure and outstanding performance observed in metal cutting operations. Several published reports suggest further that CVD-$Ti_{1-x}Al_xN$ exhibits an increased thermal stability and high temperature oxidation resistance when compared to state-of-the-art physical vapor deposited $Ti_{1-x}Al_xN$. However, the exact mechanisms underlying the oxidation of this coating system are not thoroughly understood yet. Thus within this work, the thermal stability and oxidation resistance of a powdered nanolamellar CVD-$Ti_{1-x}Al_xN$ coating have been investigated at the synchrotron radiation facility applying a novel *in-situ* experimental approach. The sample was annealed in air between 100 and 1400 °C and 2D X-ray diffraction patterns were recorded simultaneously with the differential scanning calorimetric signal. The obtained diffraction data was successively analyzed using sequential Rietveld refinement, yielding the temperature-dependent phase composition. By combining this

* Corresponding author: **E-mail:** christian.saringer@unileoben.ac.at
Tel.: +43 3842 402 4237

method with the differential scanning calorimetric data, it was possible to precisely track the onset and progress of chemical reactions. The results show that the different phases present in the sample oxidize individually, with the oxidation stability strongly depending on the Al-content. Further it was found that when $Ti_{1-x}Al_xN$ spinodally decomposes in air, the formed TiN oxidizes directly after its formation while AlN retains its chemical stability. The present work provides not only a detailed insight into the thermal stability and oxidation resistance of CVD-$Ti_{1-x}Al_xN$ but also proves the outstanding ability of the used method for analyzing metastable coatings systems.

1. Introduction

Chemical vapor deposited (CVD) $Ti_{1-x}Al_xN$ is an emerging coating material which has been the subject of intense research in the recent years as a possibly superior alternative to its well-established physical vapor deposited (PVD) counterpart. This is mainly due to the fact that in contrast to PVD-$Ti_{1-x}Al_xN$, CVD-$Ti_{1-x}Al_xN$ shows a remarkable microstructure consisting of alternating lamellae with differing chemical compositions. This lamellar structure typically comprises Al-rich face centered cubic (fcc) or hexagonal wurtzitic (w) regions, also referred to as Al(Ti)N, periodically stacked with Ti(Al)N, i.e. fcc Ti-rich domains. Typically Al contents of $x \gtrsim 0.8$ and $x \approx 0.5$ for Al(Ti)N and Ti(Al)N, respectively, are observed [1–4]. Reported values for the periodicity of these lamellae range from only a few nm [4,5] to more than 10 nm [1,2,6,7]. Up to now however, the origin of the lamellae is not clear but investigations on their origin as well as on their influence on phase stability are continuously published [3–6,8,9]. Basically, two different possible explanations for the formation of the remarkable microstructure are discussed: *i)* periodically alternating chemical reactions during deposition [1,6], as have similarly been observed for other CVD coating systems [10] and *ii)* spinodal decomposition [5].

While up to date no satisfying consensus has been found on how the lamellae are formed, published work widely agrees on the more beneficial properties of CVD-$Ti_{1-x}Al_xN$ compared to PVD-Ti_{1-}

$_xAl_xN$. Paseuth *et al.* [8] for instance, have found that CVD-$Ti_{1-x}Al_xN$ with $x \approx 0.8$ has a ten times improved lifetime during dry milling of cast iron compared to PVD-$Ti_{1-x}Al_xN$ with $x \approx 0.6$. Also, the onset temperature for the hardness decrease after annealing was higher in the CVD case. Several other publications show further, that the thermal stability of CVD-$Ti_{1-x}Al_xN$ is considerably increased compared to PVD-$Ti_{1-x}Al_xN$ [5,9,11]. Similarly, the publication of Todt *et al.* [12] suggests that the oxidation resistance of CVD-$Ti_{1-x}Al_xN$ coatings is also improved. In their work severe oxidation occurred at temperatures exceeding 1050 °C for the CVD coating compared to 900 °C in the PVD case. They mostly assign this effect to be a result of a dense oxide layer formed due to the increased amount of Al available. While in their case the CVD coating was comprised of fcc and wurtzitic $Ti_{1-x}Al_xN$ nanolamellae, Endler *et al.* [11] investigated $Ti_{0.1}Al_{0.9}N$ and $Ti_{0.18}Al_{0.82}N$ coatings which were almost exclusively fcc. They observed that these coatings retain a high oxidation resistance up to 900 °C. Additionally, no spinodal decomposition occurred in vacuum below 1200 °C for the coating with $x = 0.82$. However, in this case the coating was not specifically identified as nanolamellar.

Although several reports on the high temperature behavior of CVD-$Ti_{1-x}Al_xN$ exist, the exact processes taking place in the coating at elevated temperatures and the influence of the lamellar microstructure on the oxidation resistance remain unclear. Therefore, we have employed a new experimental approach at the P07 beamline at PETRA III in Hamburg to assess the thermal stability and oxidation resistance of a CVD-$Ti_{1-x}Al_xN$ coating. We have annealed a powdered coating in air between 100 and 1400 °C in a differential scanning calorimeter (DSC) setup, where the development of the crystallographic phases was monitored *in-situ* by X-ray diffraction (XRD). We have used the obtained temperature-dependent diffractograms for a sequential Rietveld analysis which allowed to quantitatively determine the temperature-dependent phase composition as well as lattice parameters, and correlate them with the exothermal reactions observed in the DSC signal.

The combination of DSC and XRD with a subsequent Rietveld refinement has to the best of our knowledge not been used for the investigation of the oxidation resistance of hard coatings so far. Therefore, the present work not only provides a detailed insight into the high temperature behavior of CVD-$Ti_{1-x}Al_xN$, but also demonstrates the exceptional capability of the used method for the analysis of the thermal behavior of metastable coating systems in general.

2. Experimental

The $Ti_{1-x}Al_xN$ coating investigated in this work was deposited in an industrial scale thermal CVD reactor Sucotec SCT600TH. The deposition temperature was 790 °C with a total gas flow of 101 l/min resulting in an overall pressure of 4.5 kPa. As chemical precursors $TiCl_4$, $AlCl_3$, NH_3, H_2, N_2 and Ar were used, with a ratio of the chloridic precursors $AlCl_3$:$TiCl_4$ of 6.1:1. The thickness of the $Ti_{1-x}Al_xN$ coating was ~3.7 µm with an underlying TiN baselayer having a thickness of approximately 200 nm. Cemented carbide as well as mild steel foil were used as substrates. The composition of the cemented carbide was 92 wt.-% WC, 6 wt.-% Co and 2 wt.-% mixed carbides and the substrate geometry was SNUN according to ISO 1832. In order to obtain a powder of the coating material, the coated steel foil was dissolved after deposition using nitric acid.

The coating deposited onto cemented carbide was analyzed at room temperature on a laboratory X-ray diffractometer Bruker D8 Advance in grazing incidence geometry. The used Cu-Kα radiation was collimated by a Göbel mirror and projected onto the sample at a constant incidence angle of 2°. The step-size of the performed 2θ-scan was 0.02° with a measurement time of 1.2 s per step, resulting in an overall scan speed of 1 °/min.

The *in-situ* DSC experiment coupled with synchrotron radiation XRD was carried out at the high energy materials science beamline P07 operated by the Helmholtz-Zentrum Geesthacht at the PETRA III synchrotron in Hamburg, Germany [13]. The DSC measurement was performed using

the DSC extension of the dilatometer DIL805A/D available at the synchrotron radiation beamline using two Pt-crucibles, as can be seen in Fig. 1 [14,15]. The powdered coating was placed in one crucible while the second, empty crucible was used as reference. The two crucibles were then subjected to a heating sequence in air, starting from 100 °C with a heating rate of 10 K/min up to 1400 °C. The baseline for subsequent subtraction was obtained by performing the heating cycle a second time with the already reacted powder under the assumption that no further chemical reactions take place. The energy of the X-ray beam was 87 keV, which results in a wavelength of 0.14235 Å and the sample was measured in transmission (Debye-Scherrer geometry). During the first heating cycle from 100 to 1400 °C, every ~2.1 K a frame was recorded using a 2D digital X-ray detector Perkin Elmer XRD 1621 positioned at a distance of approximately 1.9 m from the sample, resulting in 624 frames in total. The exposure time per frame was 5 s.

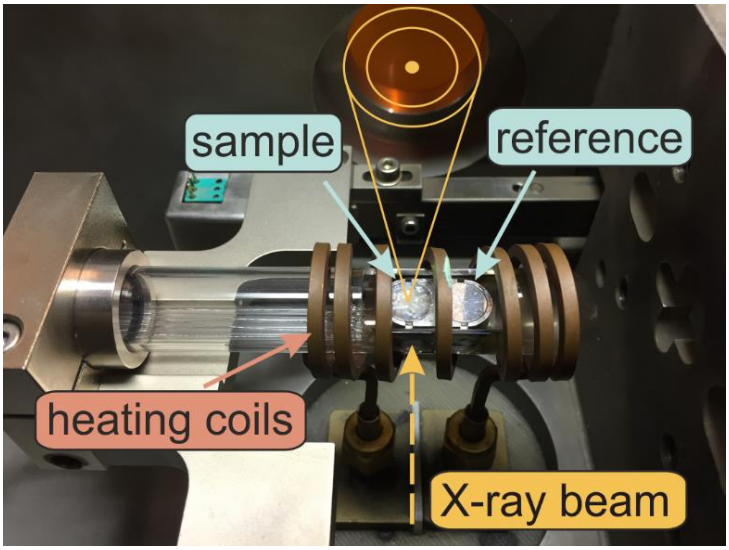

Figure 1: Experimental setup used for the *in-situ* DSC/XRD experiment at the synchrotron beamline.

The calibration and azimuthal integration of the obtained Debye-Scherrer rings to 1D diffractograms was conducted using the program Dawn2 [16]. The quantitative Rietveld refinement [17] of the subsequently obtained data was performed using the software TOPAS 6

supplied by Bruker. A semi-empirical fundamental parameter approach was employed with a LaB_6 powder (NIST 660c [18]) used for the determination and correction of the instrumental peak broadening. A sequential analysis was performed, where the results (modelled intensities, lattice parameters, …) obtained at one temperature were used as the initial parameters for the refinement at the next higher temperature step, and so on. The general criterion of convergence was a change of the R-weighted pattern (R_{wp}) value of less than 0.001 within one iteration step. A satisfying difference curve between collected data and model was used as the measure for a good fit. The crystallographic information files (cif) used for the modelling of the different phases were obtained from the Crystallography Open Database (COD) [19], see table 1.

Table1: Number code of the cif-entries in the COD used for modelling the different compounds during Rietveld refinement.

compound	**COD-code**
Al(Ti)N	1523095
Ti(Al)N	1011099
TiN baselayer	1011099
w-AlN	1010514
r-TiO_2	9004141
α-Al_2O_3	1000017
Al_2TiO_5	2107079

3. Results and discussion

X-ray diffractograms of the coating on cemented carbide and after powder production were recorded at room temperature to validate a possibly nanolamellar microstructure of the investigated CVD-$Ti_{1-x}Al_xN$ coating and to confirm that the microstructure is not altered during powdering. Both obtained X-ray diffractograms are compared in Fig. 2. Since the powder and the compact coating were measured with different photon energies (synchrotron 87 keV and laboratory radiation 8.04 keV), the d-spacing was chosen for the x-axis instead of the commonly used

diffraction angle to provide a better means of comparison. As can be seen, the coating is mainly comprised of three fcc phases for which the *hkl*-indices of the observed reflections are indicated in the figure. The peaks generally exhibiting the highest intensities in both diffractograms can be assigned to Al-rich Al(Ti)N, as their positions lie comparatively close to the standard peak positions of fcc-AlN (ICDD pdf-Nr. 00-046-1200). On the left hand sight of these peaks, an additional accompanying signal basically representing a "shoulder" can be observed. This stems from the Ti-rich Ti(Al)N and is best visible in the diffractograms of the compact coating. The third pronounced signal of an fcc phase can be recognized in the powdered sample only. The peak positions are essentially located at the standard positions of TiN (ICDD pdf-Nr. 00-038-1420) and result from the TiN baselayer. Since the baselayer is underlying the $Ti_{1-x}Al_xN$ top layer in case of the compact coating on cemented carbide, its signal is almost undetectable there. Furthermore, some minor amounts of w-AlN (ICDD pdf-Nr. 00-025-1133) are present in the coating. A quantitative Rietveld analysis of the data acquired for the powder before any chemical reactions or spinodal decomposition have taken place, i.e. averaged compositions obtained below 500 °C, yielded a phase composition of approximately 58 wt.-% Al(Ti)N, 28 wt.-% Ti(Al)N, 12 wt.-% TiN as well as minor wurtzitic amounts $\lesssim$ 2 wt.-%. Other peaks present either belong to the cemented carbide substrate in the case of the compact coating on cemented carbide or to the Pt-crucible used to contain the powder during the DSC measurement at P07. However, as they do not have any significance for the evaluation they were ignored during the subsequent quantitative phase analysis. Additional observable low-intensity peaks in the synchrotron radiation case, as for instance at 4.1 Å, stem from higher order reflections resulting from the single crystalline Si monochromators.

The diffractograms presented in Fig. 2 correspond well with published diffractograms for nanolamellar CVD-$Ti_{1-x}Al_xN$ coatings [2,4]. In order to further confirm the nanolamellar microstructure, however, the coating deposited on cemented carbide was additionally investigated

using transmission electron microscopy. There indeed, nanolamellae could be observed in the bright field image. Moreover, $Ti_{0.2}Al_{0.8}N$ deposited with the same deposition parameters were investigated already for which also a nanolamellar structure was found [4]. It is evident from Fig. 2 that the phases present are the same in the coating deposited on cemented carbide and in the powdered case. Hence it can be concluded, that the powder investigated at the synchrotron will behave in a similar way to a compact coating.

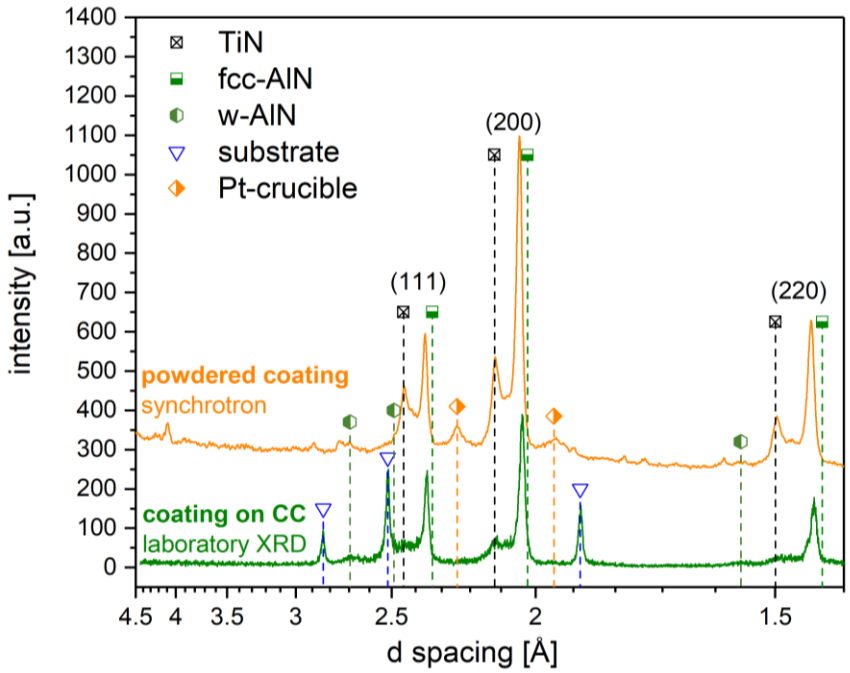

Figure 2: Room temperature X-ray diffractograms of the powder acquired at the synchrotron radiation facility and the compact coating on cemented carbide (CC) recorded using a laboratory diffractometer in grazing incidence geometry (incidence angle 2°).

In addition to the phase composition, a Rietveld analysis provides the lattice parameter of the refined phases, which are approximately 4.09 and 4.17 Å for Al(Ti)N and Ti(Al)N, respectively, at room temperature. According to ref. [6] these lattice parameters correspond to compositions of $Ti_{0.1}Al_{0.9}N$ and $Ti_{0.5}Al_{0.5}N$. These compositions are in good agreement with reported ones for the Al-rich and Ti-rich fcc lamellae [4–6,20].

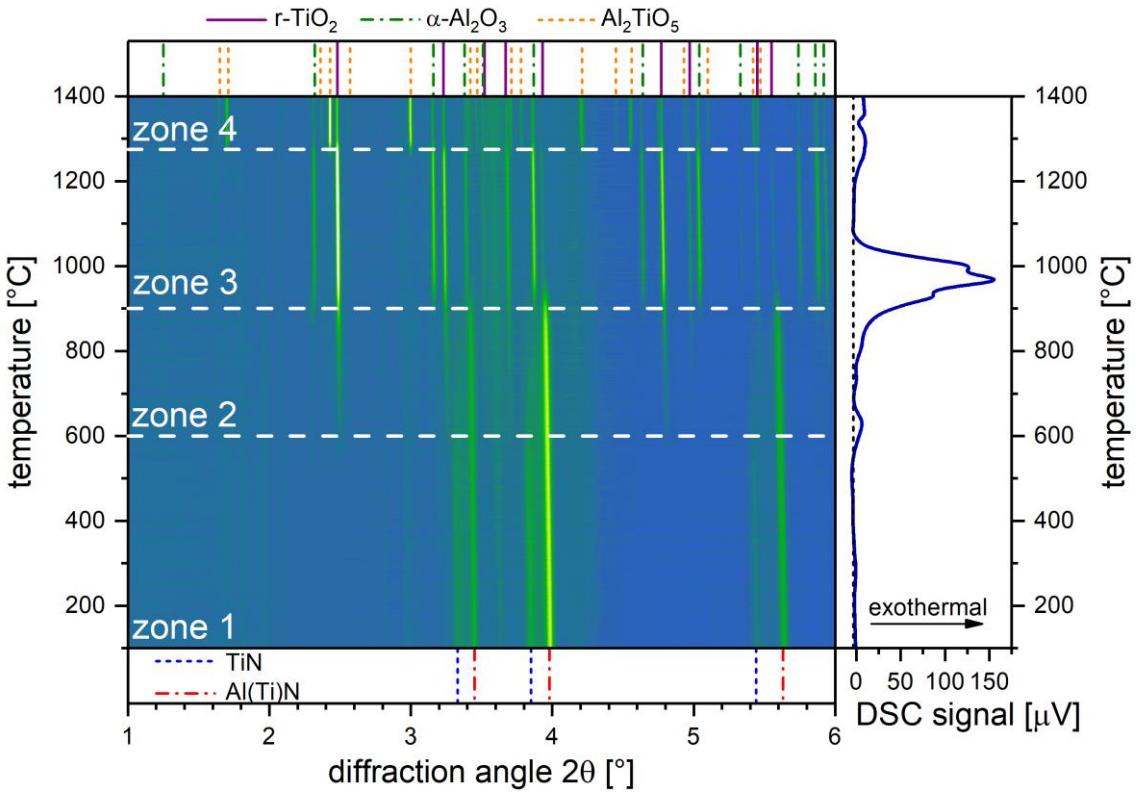

Figure 3: XRD-phase plot acquired by integrating the 2D XRD data obtained during the *in-situ* synchrotron radiation experiment and DSC signal (baseline subtracted). The positions of the Bragg-reflections of the different phases are indicated by vertical lines at the top and bottom of the phase plot.

In order to obtain data suitable for Rietveld analysis, i.e. 1D diffractograms similar to the ones presented in Fig. 2, the 2D Debye-Scherrer rings acquired at P07 for all temperatures were azimuthally integrated over the complete angular range, i.e. from 0 to 360°. The results of the integration are presented in Fig. 3 in the shape of a 2D contour plot, i.e. intensity over diffraction angle and temperature, usually referred to as phase plot, along with the obtained DSC signal on the right. The phase plot can be divided into four distinct temperature zones with different phases present. The borders between these zones are indicated by horizontal, dashed lines and are characterized by the appearance of new phases. As can be noticed, these lines correspond to peaks in the DSC signal, i.e. the occurrence of exothermal reactions. In zone 1 (100 °C – 600 °C), mainly

two fcc phases are visible which are related to the signals of the Al(Ti)N and the TiN baselayer. The Ti(Al)N can only be recognized as an indistinct intensity between those of the other two phases. A slight shift of the signals to lower angles with increasing temperature is observable in the whole temperature range. Since lower diffraction angles correspond to increased lattice parameters this can be attributed to the thermal expansion of the lattices. At approximately 600 °C a first chemical reaction characterized by the disappearance of the TiN signal and the appearance of rutile titania (r-TiO_2) marks the border to zone 2. A comparatively small exothermal peak in the DSC signal is also detectable in the same temperature range. This border can be allocated to the oxidation of the TiN baselayer. At the same time, however, the phases including Al, namely Al(Ti)N and Ti(Al)N retain their chemical stability.

Upon further increasing the temperature to values above approximately 900 °C (border to zone 3) α-alumina (α-Al_2O_3) is formed while Al(Ti)N vanishes together with the weak signal of Ti(Al)N. Simultaneously, the intensity of r-TiO_2 is increased. Also, a strong exothermal signal occurs together with this change of the present phases in the DSC. These observations can be connected to the oxidation of the $Ti_{1-x}Al_xN$ coating. At a temperature of ~1275 °C (border to zone 4) aluminum titanate (Al_2TiO_5) forms at the cost of r-TiO_2 and α-Al_2O_3. However, this reaction does not take place completely and some r-TiO_2 and α-Al_2O_3 are retained up to 1400 °C.

In order to more precisely determine the temperature dependence of the chemical reactions and to quantify the phases present, a sequential Rietveld refinement was performed for all XRD data recorded over the whole investigated temperature range. Figure 4 displays the integrated diffractograms and refined models for four different temperatures, representing typical diffraction data for each of the four observed temperature zones. The red bottom lines in the graphs show the differences between measured and modelled intensities, their visual appearances were used as the main criterion for satisfying fits.

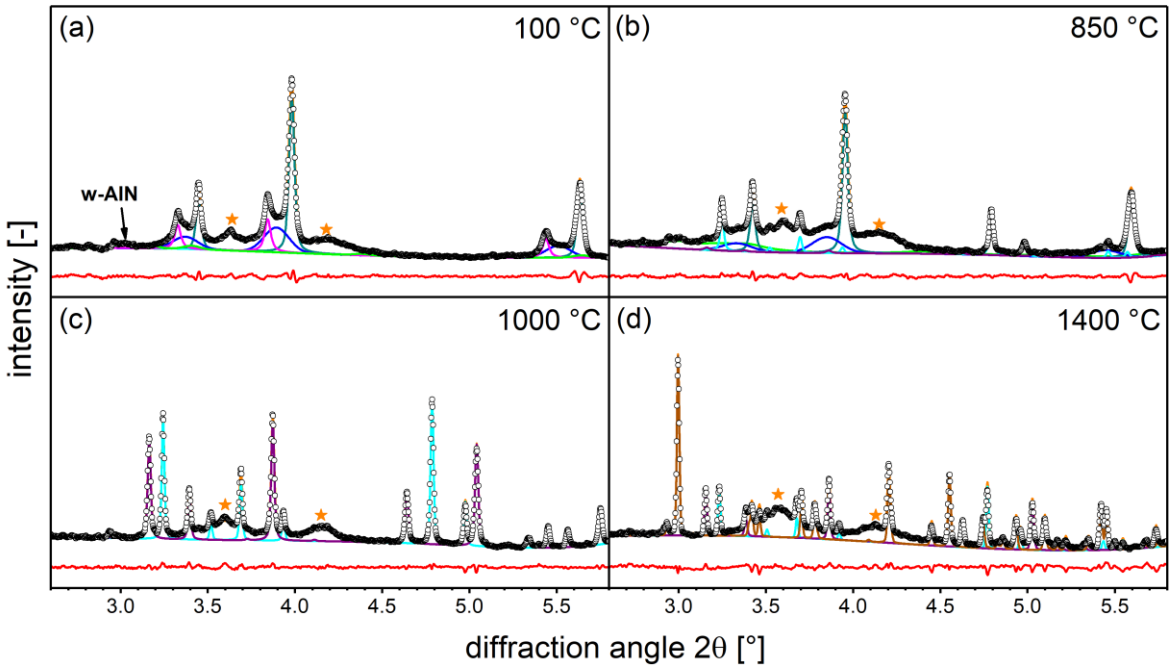

Figure 4: 1D integrated diffractograms obtained during the annealing procedure for temperatures of (a) 100 °C, (b) 850 °C, (c) 1000 °C and (d) 1400 °C, representing one typical diffractogram for each of the four observed zones. The corresponding models refined by the Rietveld method are also shown. Measured data is represented by dots (○) and the modelled intensity and difference curves are in orange ( ) and red ( ), respectively. The modelled individual phases are Al(Ti)N ( ), Ti(Al)N ( ), TiN baselayer ( ), wurtzitic AlN ( ), r-TiO_2 ( ), α-Al_2O_3 ( ) and Al_2TiO_5 ( ). The signal resulting from the Pt crucible was corrected for by two additionally refined peaks at approximately 3.6 and 4.2° (★). However, the two modelled peaks are not displayed in the figure.

From the modelled curves in Fig. 4a it is evident that the pronounced fcc "double peaks" observed in Figs. 2 and 3 are indeed comprised of three individual phases which correspond to fcc-Al(Ti)N, fcc-Ti(Al)N and the TiN baselayer. While the TiN baselayer and Al(Ti)N show sharp Bragg-reflections, the reflections stemming from Ti(Al)N are considerably broader, which is attributed to the domain size effect [21], i.e. a smaller size of coherently diffracting domains of the Ti(Al)N

phase. This correlates well with the typically observed reduced lamella thickness of Ti(Al)N when compared to Al(Ti)N [1,2,4,4–6,20]. In Fig. 4b the baselayer is completely oxidized and a considerable amount of r-TiO_2 has formed. Also, the intensity of Ti(Al)N has somewhat decreased. Figure 4c shows a completely oxidized coating consisting of r-TiO_2 and α-Al_2O_3. In zone 4 eventually some of the r-TiO_2 and α-Al_2O_3 has reacted to Al_2TiO_5 (Fig. 4d). As can be seen, the presented figures proof an excellent agreement between model and measurement.

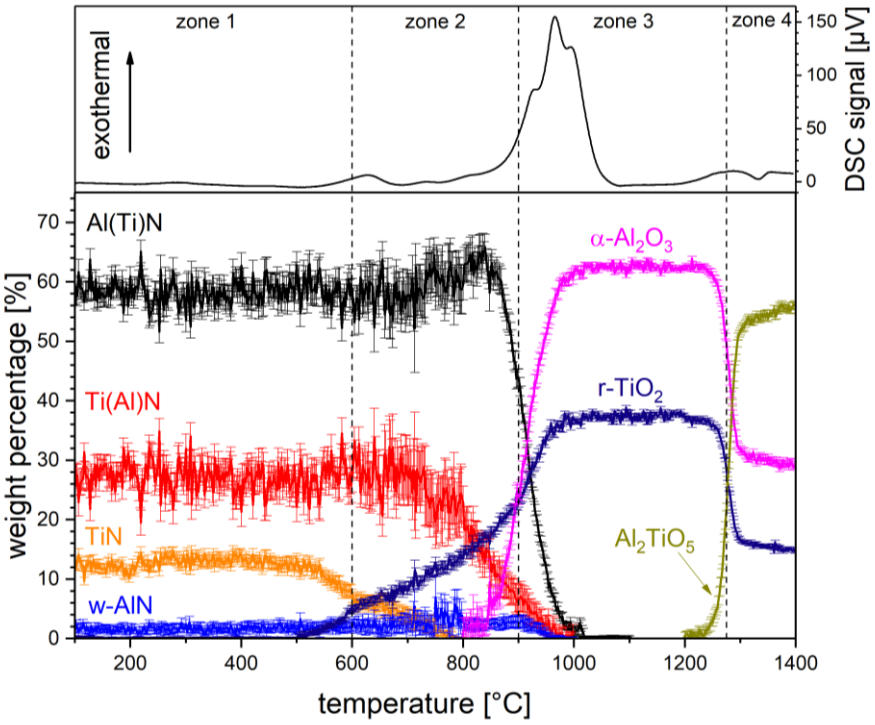

Figure 5: Phase composition obtained by the sequential Rietveld analysis in combination with the DSC signal (baseline subtracted) as a function of the temperature. The presented error bars are the estimated standard deviations of the weight percentage obtained from TOPAS 6.

By performing a Rietveld analysis of the X-ray diffractograms acquired during annealing and displaying the results as a function of the temperature, one can precisely follow and analyze phase transformations and chemical reactions. Figure 5 shows the quantitative phase composition during the oxidation cycle of the investigated CVD-$Ti_{1-x}Al_xN$ coating obtained from the mentioned

Rietveld analysis. Additionally, an animation of the *in-situ* annealing experiment is available as supplementary material online which shows the progress of the experiment and the subsequently obtained results. At first glance it becomes obvious that the phases and their amounts strongly vary with increasing temperature and three pronounced reactions can be determined. These correspond to the borders between the four observed zones, as already discussed. However, in contrast to the phase plot presented in Fig. 2, a more detailed insight is gained, especially concerning the onset and progress of chemical reactions.

During annealing between 100 and 550 °C in air, the phase composition essentially remains constant. The relatively large error bars especially for Ti(Al)N and Al(Ti)N result from the fact that there are three fcc phases present which have strongly overlapping signals (compare Fig. 4a). At ~550 °C a first change of the phase composition can be recognized: The amount of TiN starts to decrease, while at the same time r-TiO_2 is formed. Simultaneously, an exothermal peak in the DSC signal can be recognized. This temperature corresponds well with results of other researchers who reported an oxidation temperature of pure TiN coatings between 550 and 600 °C [22–24]. Therefore, these observations are related to the oxidation of the baselayer. This reaction would, however, most probably not occur in a compact sample deposited onto a cemented carbide substrate. As the TiN would underlie the $Ti_{1-x}Al_xN$ in that case, its oxidation could only start after the top layer is completely oxidized eventually allowing the oxygen to reach the base layer.

A further increase of the temperature is characterized by the oxidation of the baselayer until approximately 680 °C. At this point the amount of Ti(Al)N begins to decrease. However, only a minor exothermal peak, considerably smaller than the peak observed for the oxidation of the TiN, is present in the DSC signal. At the same time, the amount of Al(Ti)N increases somewhat to 65 wt.-%. This observation can best be apprehended when assessing the temperature-dependent lattice parameters of the three fcc phases, shown in Fig. 6. As can be seen, the lattice parameters of the

phases a_{ph} are influenced by the amount of Al in the fcc TiN-based lattice, since $a_{TiN} > a_{Ti(Al)N} > a_{Al(Ti)N}$. Also, a_{ph} generally increase with temperature as a result of the thermal expansion of the lattices. However, at ~680 °C a sudden increase of $a_{Ti(Al)N}$ occurs. This is typical for the spinodal

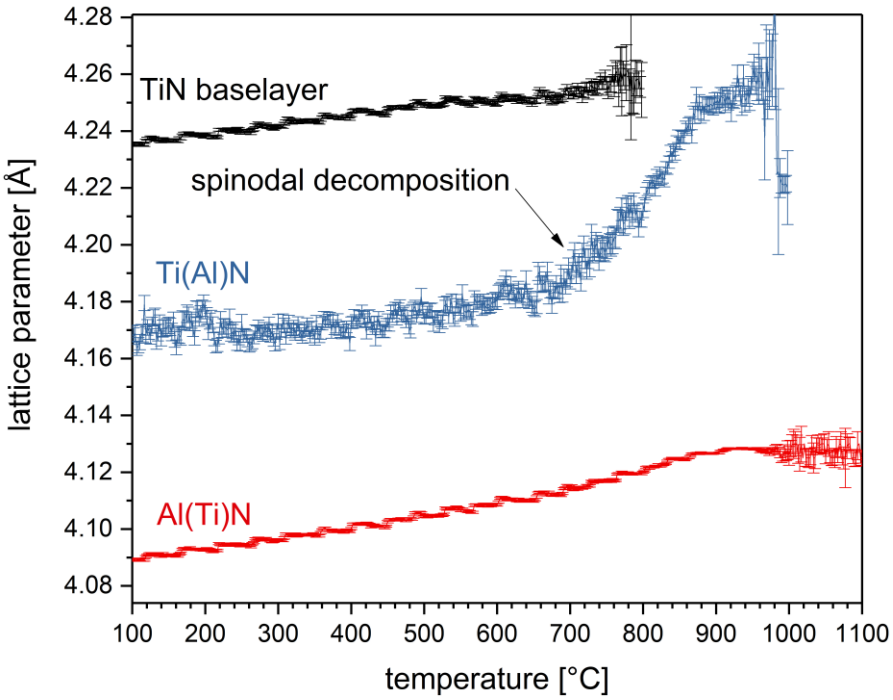

Figure 6: Lattice parameters of the three observed face centered cubic phases Al(Ti)N, Ti(Al)N and the TiN baselayer obtained by Rietveld analysis as a function of the temperature. The presented error bars are the estimated standard deviations of the lattice parameter supplied by TOPAS 6. The increase in error at the highest temperatures is a result of the fact that when the intensity contributions of the individual phases decrease to approximately zero, also their lattice parameters become more difficult to refine.

decomposition observed for metastable fcc-$Ti_{1-x}Al_xN$ into fcc-TiN and fcc-AlN [25]. The loss of Al in Ti(Al)N due to spinodal decomposition results in an increase of the lattice parameter towards the value of TiN [4,26]. The formation of fcc-AlN on the other hand results in an apparent increase of the amount of Al(Ti)N. Spinodal decomposition is completed at ~880 °C, above which the lattice parameter of Ti(Al)N has reached the approximate value of TiN. Recently, we have

investigated the spinodal decomposition of an equivalent coating annealed in vacuum [4]. There, we found the onset of spinodal decomposition at temperatures above 900 °C. Also other reports indicate that the onset of spinodal decomposition of CVD-$Ti_{1-x}Al_xN$ usually occurs at higher temperatures than observed in this work [2,5,8]. Consequently, it can be concluded that the present oxygen has an influence not only on the chemical stability of the coating (i.e. the formation of oxidic reaction products), but also on the phase stability of the Ti-rich fcc phase. This is in good agreement with the findings of Endler et al. [11], who also found a higher stability of CVD-$Ti_{1-x}Al_xN$ when annealed in vacuum (1200 °C) compared to air (900 °C). Furthermore, some exothermal background is visible above 800 °C in the DSC signal. This, in combination with the permanent increase of the amount of r-TiO_2 with temperature, indicates that the TiN formed during spinodal decomposition oxidizes directly after its formation.

fcc-AlN is metastable and consequently transforms to stable w-AlN at elevated temperatures [25]. The modelled intensity of w-AlN was somewhat difficult to accurately refine during the Rietveld analysis because most of its peak positions coincide with those of the fcc phases, except for one peak at approximately 3°. Exactly in this region, however, a higher order reflection resulting from the Si monochromator is located (see Fig. 4a). Therefore, the error of the amount of w-AlN is relatively large, especially between 700 and 800 °C. Above 800 °C its amount shows a slight increase with temperature to approximately 3 wt.-% and it can therefore be refined well in this region. This indicates that indeed the formed fcc-AlN transforms to w-AlN. Also a small additional peak in the DSC signal can be observed between 800 and 900 °C which most probably results from this transformation along with a potential recovery of the fcc phases [4,27].

The exact onset temperature of the oxidation of the Ti(Al)N is hard to determine from Fig. 5 as it is superimposed by spinodal decomposition. However, clearly oxidation of this phase takes already place at 800 °C which is evidenced by the fact that above this temperature the TiN baselayer has

completely reacted, but the amount of r-TiO_2 is nevertheless increasing. Al(Ti)N on the other hand clearly starts to oxidize at ~850 °C which coincides with the first occurrence of α-Al_2O_3.

Apparently, the main peak in the DSC signal positioned between 860 and 1080 °C corresponds to the oxidation of the actual $Ti_{1-x}Al_xN$ coating. It is comprised of three individual contributions and the three observed peaks can be assigned due to the Al-content in the individual phases. Ti(Al)N has a lower Al-content compared to Al(Ti)N. Therefore, the first peak is related to the oxidation of Ti(Al)N, while the second one corresponds to the oxidation of Al(Ti)N. This conclusion is additionally substantiated by the fact that the size of the peaks in the DSC signal corresponds to the amount of the respective phases. Al(Ti)N constitutes the largest part of the coating and its oxidation consequently releases the highest amount of energy, resulting in the highest peak in the DSC signal. In Fig. 5 it can be seen that w-AlN shows the highest resistance to oxidation since it is stable up to 900 °C. This corresponds well with already reported results where it was found that due to the higher amount of Al available in wurtzitic $Ti_{1-x}Al_xN$ coatings, they show a better oxidation resistance compared to purely cubic coatings [2,28]. Consequently, the third contribution results from the oxidation of w-AlN. This peak is small compared to the second one which is in agreement with the small amount of w-AlN present in the coating.

Eventually, above 1000 °C the whole coating has reacted to r-TiO_2 and α-Al_2O_3 with respective phase fractions of 38 and 62 wt.-%. No anatase TiO_2 is observed during the whole annealing process and thus the coating obviously directly transforms to rutile instead of an occasionally observed intermediate reaction step to metastable anatase [29–32]. The much higher exothermal peak of the oxidation of the coating compared to that of spinodal decomposition in the DSC signal corresponds well with the report by Chen *et al.* [28]. Similarly, they found an approximately 100-times increased signal when comparing oxidation and spinodal decomposition in the DSC. However, in their case the individual contribution of spinodal decomposition and oxidation were

not distinguishable within one DSC measurement due to the overlap of signals and annealing cycles were performed separately in air and vacuum. This demonstrates the good resolution of the DSC at the P07 beamline where both contributions could be discerned within one single measurement by the aid of a sequential Rietveld analysis.

Upon further increasing the temperature, no change in the phase composition occurs until at ~1250 °C Al_2TiO_5 starts to form at the cost of r-TiO_2 and α-Al_2O_3. Al_2TiO_5 is the thermodynamically stable high temperature phase of a 1/1-mixture of TiO_2/Al_2O_3 [33]. This phase has also been observed during the annealing of PVD-$Ti_{1-x}Al_xN$-based hard coatings [28,31,32,34]. Its formation is accompanied by another exothermal peak in the DSC signal. At the highest temperatures investigated, r-TiO_2 and α-Al_2O_3 further react to Al_2TiO_5, however, at a much slower rate than during the main transformation around 1275 °C. This is in good agreement with the results reported by Freudenberg and Mocellin [35,36], who have found two stages of the reaction of powdered α-Al_2O_3 and TiO_2 (anatase and rutile) to Al_2TiO_5. One fast initial reaction step followed by a second step with a reduced rate. The decreased reaction speed was attributed to the limitation of reactant diffusion through the formed Al_2TiO_5 reacted layer.

Figure 7 shows the DSC signal, summarizing the evolution of the CVD-$Ti_{1-x}Al_xN$ coating investigated within the *in-situ* synchrotron radiation experiment. It demonstrates that by the use of the presented method we were able to correlate all significant exothermal peaks observed during the measurement with reactions taking place in the coating. In addition, the spinodal decomposition could be clearly separated from the oxidation in the DSC signal, although it shows only a very minor signal in comparison. This was only possible by thoroughly analyzing the XRD data with respect to phase composition and lattice parameters using a sequential Rietveld refinement.

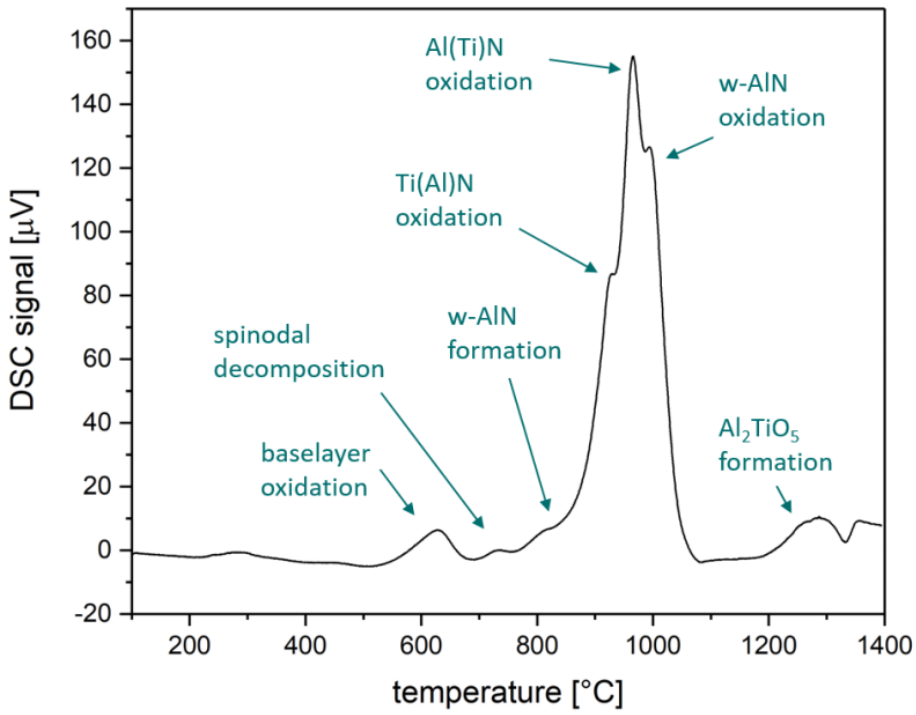

Figure 7: DSC signal (background subtracted) obtained at the synchrotron radiation facility with all exothermal peaks assigned to either chemical reactions or phase transformations.

As a final point it needs to be discussed that results obtained for a solid coating on a substrate might to some extent differ from the results gained for powders. In contrast to a coating on a substrate a powder has a higher surface to volume ratio and does not contain residual stresses. Due to the smaller amount of surface that is exposed to air during annealing in the compact coating the kinetics of the oxidation reaction are therefore somewhat retarded leading to longer oxidation times and to increased finish temperatures of the oxidational reactions. In contrast, the onset temperatures, the specific type of reaction and the phase evolution are the same. These mainly depend on the elemental composition of the individual phases, i.e. the Al content in this case, and not on the exposed surface. Also, since the TiN baselayer is underlying the $Ti_{1-x}Al_xN$ top layer in the compact coating, its oxidation starts only after the top layer is completely oxidized. At the high temperatures

investigated the residual stress relaxes having therefore no influence on the oxidation behavior even in the compact coating. These conclusions evidence that important implications valid for both cases can be obtained from powders.

4. Conclusion

Within this work a powdered nanolamellar $Ti_{1-x}Al_xN$ coating on a TiN baselayer produced by chemical vapor deposition (CVD) was investigated employing a novel approach of combined differential scanning calorimetry (DSC) and synchrotron radiation X-ray diffraction (XRD). The powder sample was investigated in air between 100 and 1400 °C and the obtained XRD data was analyzed using sequential Rietveld refinement. This procedure yielded the temperature-dependent evolution of the phase composition as well as lattice parameters of the present phases. By correlating the obtained data with the DSC signal a deep insight into the thermal stability and oxidation resistance of CVD-$Ti_{1-x}Al_xN$ was obtained providing the following main conclusions:

i. The high resolution at the synchrotron radiation facility of both XRD and DSC allowed to discern the influences of spinodal decomposition and oxidation on the phase composition of the coating. The onset of spinodal decomposition found here is approximately 200 K lower than observed before for vacuum annealed CVD-$Ti_{1-x}Al_xN$. This implies that the oxygen present in ambient atmosphere has a negative influence on the thermal phase stability of fcc-$Ti_{1-x}Al_xN$.
ii. When TiN is formed during the spinodal decomposition of $Ti_{1-x}Al_xN$ it oxidizes to rutile TiO_2 directly after its formation due to the loss of the protective Al in the lattice.
iii. The individual phases in the investigated coating system, i.e. the TiN baselayer, the Ti-rich Ti(Al)N, the Al-rich Al(Ti)N and the wurtzitic (w-)AlN start to oxidize independently at different temperatures. The sequence of the oxidation onset temperatures is TiN < Ti(Al)N < Al(Ti)N < w-AlN, which evidences the positive influence of Al on the

oxidation resistance. However, this also indicates that the observed higher oxidation resistance of CVD-$Ti_{1-x}Al_xN$ compared to the physical vapor deposited $Ti_{1-x}Al_xN$ does not result from the lamellar microstructure, but is rather caused by the increased average amount of Al present.

In addition to the results obtained on the thermal stability of CVD-$Ti_{1-x}Al_xN$, the present work demonstrates the exceptional capability of the used experimental and analytical approach to improve the understanding of the temperature-dependent evolution of metastable coating systems in general.

5. Acknowledgements

The financial support by the Austrian Federal Ministry for Digital and Economic Affairs and the National Foundation for Research, Technology and Development is gratefully acknowledged. The authors also gratefully acknowledge the financial support under the scope of the COMET program within the K2 Center “Integrated Computational Material, Process and Product Engineering (IC-MPPE)” (Project No 859480). This program is supported by the Austrian Federal Ministries for Transport Innovation and Technology (BMVIT) and for Digital and Economic Affairs (BMDW), represented by the Austrian research funding association (FFG), and the federal states of Styria, Upper Austria and Tyrol. We would also like to thank Gabriele Felber from the Erich Schmid Institute of Materials Science of the Austrian Academy of Sciences for the preparation of the TEM-lamella.

6. References

[1] J. Keckes, R. Daniel, C. Mitterer, I. Matko, B. Sartory, A. Koepf, R. Weißenbacher, R. Pitonak, Self-organized periodic soft-hard nanolamellae in polycrystalline TiAlN thin films, Thin Solid Films 545 (2013) 29–32. https://doi.org/10.1016/j.tsf.2013.08.001.

[2] J. Todt, J. Zalesak, R. Daniel, R. Pitonak, A. Köpf, R. Weißenbacher, B. Sartory, C. Mitterer, J. Keckes, Al-rich cubic $Al_{0.8}Ti_{0.2}N$ coating with self-organized nano-lamellar microstructure, Surf. Coat. Tech. 291 (2016) 89–93. https://doi.org/10.1016/j.surfcoat.2016.02.027.

[3] A. Paseuth, A. Miura, K. Tadanaga, K. Yamagata, Thermal stability of Al-rich c-$Al_xTi_{1-x}N$ coatings prepared by LP-CVD, Proc. 19th Int. Plansee Semin., Reutte HM 49 (2017) 1–11.

[4] M. Tkadletz, C. Hofer, C. Wüstefeld, N. Schalk, M. Motylenko, D. Rafaja, H. Holzschuh, B. Sartory, C. Mitterer, C. Czettl, Temperature-driven microstructural evolution of nanolamellar fcc-$Ti_{1-x}Al_xN$ grown by chemical vapor deposition, submitted for publication to Acta Materialia.

[5] A. Paseuth, K. Yamagata, A. Miura, M. Higuchi, K. Tadanaga, Deposition and analysis of Al-rich c-$Al_xTi_{1-x}N$ coating with preferred orientation, J. Am. Ceram. Soc. 100 (2017) 343–353. https://doi.org/10.1111/jace.14549.

[6] J. Zalesak, D. Holec, I. Matko, M. Petrenec, B. Sartory, N. Koutná, R. Daniel, R. Pitonak, J. Keckes, Peculiarity of self-assembled cubic nanolamellae in the TiN/AlN system: Epitaxial self-stabilization by element deficiency/excess, Acta Mater. 131 (2017) 391–399. https://doi.org/10.1016/j.actamat.2017.04.009.

[7] J. Zalesak, J. Todt, R. Pitonak, A. Köpf, R. Weißenbacher, B. Sartory, M. Burghammer, R. Daniel, J. Keckes, Combinatorial refinement of thin-film microstructure, properties and process conditions: Iterative nanoscale search for self-assembled TiAlN nanolamellae, J. Appl. Crystallogr. 49 (2016) 2217–2225. https://doi.org/10.1107/S1600576716017258.

[8] A. Paseuth, Y. Kido, S. Imamura, K. Yamagata, A. Miura, K. Tadanaga, Thermal stability and cutting performance of Al-rich cubic $Al_xTi_{1-x}N$ coating prepared by low-pressure chemical vapour deposition, J. Ceram. Soc. Jpn. 125 (2017) 913–918. https://doi.org/10.2109/jcersj2.17152.

[9] F. Mercier, H. Shimoda, S. Lay, M. Pons, E. Blanquet, Reactive chemical vapor deposition of heteroepitaxial $Ti_{1-x}Al_xN$ films, Cryst. Eng. Comm. 20 (2018) 1711–1715. https://doi.org/10.1039/C7CE02129A.

[10] K. Bartsch, A. Leonhardt, E. Wolf, Deposition of multilayer hard coatings using kinetically controlled chemical vapour deposition processes, Surf. Coat. Tech. 54-55 (1992) 193–197. https://doi.org/10.1016/S0257-8972(09)90049-4.

[11] I. Endler, M. Höhn, M. Herrmann, R. Pitonak, S. Ruppi, M. Schneider, H. van den Berg, H. Westphal, Novel aluminum-rich $Ti_{1-x}Al_xN$ coatings by LPCVD, Surf. Coat. Tech. 203 (2008) 530–533. https://doi.org/10.1016/j.surfcoat.2008.04.098.

[12] J. Todt, R. Pitonak, A. Köpf, R. Weißenbacher, B. Sartory, M. Burghammer, R. Daniel, T. Schöberl, J. Keckes, Superior oxidation resistance, mechanical properties and residual stresses of an Al-rich nanolamellar $Ti0_{.05}Al_{0.95}N$ coating prepared by CVD, Surf. Coat. Tech. 258 (2014) 1119–1127. https://doi.org/10.1016/j.surfcoat.2014.07.022.

[13] N. Schell, A. King, F. Beckmann, T. Fischer, M. Müller, A. Schreyer, The High Energy Materials Science Beamline (HEMS) at PETRA III, Mater. Sci. Forum 772 (2013) 57–61. https://doi.org/10.4028/www.scientific.net/MSF.772.57.

[14] P. Staron, T. Fischer, T. Lippmann, A. Stark, S. Daneshpour, D. Schnubel, E. Uhlmann, R. Gerstenberger, B. Camin, W. Reimers, E. Eidenberger, H. Clemens, N. Huber, A. Schreyer, In situ experiments with synchrotron high-energy X-rays and neutrons, Adv. Eng. Mater. 13 (2011) 658–663. https://doi.org/10.1002/adem.201000297.

[15] J. Medina, P. Pérez, G. Garces, D. Tolnai, A. Stark, N. Schell, P. Adeva, Microstructural changes in an extruded Mg Zn Y alloy reinforced by quasicrystalline I-phase by small additions of calcium, manganese and cerium-rich mischmetal, Mater. Charact. 118 (2016) 186–198. https://doi.org/10.1016/j.matchar.2016.05.019.

[16] M. Basham, J. Filik, M.T. Wharmby, P.C.Y. Chang, B. El Kassaby, M. Gerring, J. Aishima, K. Levik, B.C.A. Pulford, I. Sikharulidze, D. Sneddon, M. Webber, S.S. Dhesi, F. Maccherozzi, O. Svensson, S. Brockhauser, G. Náray, A.W. Ashton, Data Analysis WorkbeNch (DAWN), J. Synchrotron Radiat. 22 (2015) 853–858. https://doi.org/10.1107/S1600577515002283.

[17] R.A. Young, The Rietveld Method, Oxford University Press, Oxford, New York, 1993.

[18] NIST 660c certificate, https://www-s.nist.gov, accessed December 2018.

[19] Crystallography Open Database, http://www.crystallography.net, accessed December 2018.

[20] C. Czettl, U. Schleinkofer, F. Schedle, C. Wolf, M. Lechleitner, H. Holzschuh, W. Bürgin, CVD TiAlN - development and challenges for use in mass production, Proc. 19th Int. Plansee Semin., Reutte HM 45 (2017) 1–13.

[21] P. Scherrer, Bestimmung der Größe und der inneren Struktur von Kolloidteilchen mittels Röntgenstrahlen, Nachr. Ges. Wiss. Göttingen 1918 (1918) 98–100.

[22] W.-D. Münz, Titanium aluminum nitride films: A new alternative to TiN coatings, J. Vac. Sci. Technol. A 4 (1986) 2717–2725. https://doi.org/10.1116/1.573713.

[23] I. Milošev, H.-H. Strehblow, B. Navinšek, M. Metikoš-Huković, Electrochemical and thermal oxidation of TiN coatings studied by XPS, Surf. Interface Anal. 23 (1995) 529–539. https://doi.org/10.1002/sia.740230713.

[24] C.W. Kim, K.H. Kim, Anti-oxidation properties of TiAlN film prepared by plasma-assisted chemical vapor deposition and roles of Al, Thin Solid Films 307 (1997) 113–119. https://doi.org/10.1016/S0040-6090(97)00212-5.

[25] A. Hörling, L. Hultman, M. Odén, J. Sjölén, L. Karlsson, Thermal stability of arc evaporated high aluminum-content $Ti_{1-x}Al_xN$ thin films, J. Vac. Sci. Technol. A 20 (2002) 1815–1823. https://doi.org/10.1116/1.1503784.

[26] R. Rachbauer, S. Massl, E. Stergar, D. Holec, D. Kiener, J. Keckes, J. Patscheider, M. Stiefel, H. Leitner, P.H. Mayrhofer, Decomposition pathways in age hardening of Ti-Al-N films, J. Appl. Phys. 110 (2011) 23515. https://doi.org/10.1063/1.3610451.

[27] P.H. Mayrhofer, A. Hörling, L. Karlsson, J. Sjölén, T. Larsson, C. Mitterer, L. Hultman, Self-organized nanostructures in the Ti–Al–N system, Appl. Phys. Lett. 83 (2003) 2049–2051. https://doi.org/10.1063/1.1608464.

[28] L. Chen, J. Paulitsch, Y. Du, P.H. Mayrhofer, Thermal stability and oxidation resistance of Ti-Al-N coatings, Surf. Coat. Tech. 206 (2012) 2954–2960. https://doi.org/10.1016/j.surfcoat.2011.12.028.

[29] D.A.H. Hanaor, C.C. Sorrell, Review of the anatase to rutile phase transformation, J. Mater. Sci. 46 (2011) 855–874. https://doi.org/10.1007/s10853-010-5113-0.

[30] M. Pfeiler, J. Zechner, M. Penoy, C. Michotte, C. Mitterer, M. Kathrein, Improved oxidation resistance of TiAlN coatings by doping with Si or B, Surf. Coat. Tech. 203 (2009) 3104–3110. https://doi.org/10.1016/j.surfcoat.2009.03.036.

[31] Y.X. Xu, L. Chen, F. Pei, J.L. Yue, Y. Du, Thermal stability and oxidation resistance of V-alloyed TiAlN coatings, Ceram. Int. 44 (2018) 1705–1710. https://doi.org/10.1016/j.ceramint.2017.10.100.

[32] B. Grossmann, M. Tkadletz, N. Schalk, C. Czettl, M. Pohler, C. Mitterer, High-temperature tribology and oxidation of $Ti_{1-x-y}Al_xTa_yN$hard coatings, Surf. Coat. Tech. 342 (2018) 190–197. https://doi.org/10.1016/j.surfcoat.2018.02.062.

[33] S. Hoffmann, S.T. Norberg, M. Yoshimura, Structural models for intergrowth structures in the phase system Al_2O_3–TiO_2, J. Solid State Chem. 178 (2005) 2897–2906. https://doi.org/10.1016/j.jssc.2005.07.001.

[34] M. Golizadeh, K.A. Kuptsov, N.V. Shvyndina, D.V. Shtansky, Multilayer SiBCN/TiAlSiCN and AlO_x/TiAlSiCN coatings with high thermal stability and oxidation resistance, Surf. Coat. Tech. 319 (2017) 277–285. https://doi.org/10.1016/j.surfcoat.2017.04.016.

[35] B. Freudenberg, A. Mocellin, Aluminum titanate formation by solid-state reaction of fine Al_2O_3 and TiO_2 powders, J. Am. Ceram. Soc. 70 (1987) 33–38. https://doi.org/10.1111/j.1151-2916.1987.tb04849.x.

[36] B. Freudenberg, A. Mocellin, Aluminum titanate formation by solid-state reaction of coarse Al_2O_3 and TiO_2 powders, J. Am. Ceram. Soc. 71 (1988) 22–28. https://doi.org/10.1111/j.1151-2916.1988.tb05755.x.